PCB PIEZOTRONICS

Field Evaluations of a Damped MEMS Shock Sensor

Field Evaluations
of a Damped MEMS Shock Sensor

Abstract

Results from pyrotechnic, penetration and metal-to-metal impact field evaluations are presented which prove the performance of a new piezoresistive (PR) shock accelerometer. The micro-electromechanical systems (MEMS) sensor incorporates sufficient squeeze-film damping to reduce resonant amplification during violent events by orders of magnitude over conventional undamped PR MEMS designs. Such damping enhances survivability and reduces the need for filtration, whether mechanical or electrical, to block unwanted high frequency output. Analysis of results shows that the frequency response of the new sensor is more than adequate to measure the rigid body motion and meaningful structural modes resulting from most shock events.

Introduction

Evaluation testing has begun on a family of piezoresistive shock accelerometers for extreme shock applications. For this family a unique 20kG silicon MEMS sensor was developed incorporating stops and damping. Discussed in this paper are several sets of results: one with a Hopkinson bar, two with gun-launched penetration, a test using pyrotechnics, and two metal-on-metal hammer tests, all of which confirm the beneficial effect of damping in shock environments. Most tests were performed side-by-side with legacy MEMS devices (used since the 1980's), that are undamped, unstopped, and have high resonance frequencies. The tests compared the sensors and the packaging in which they were housed.

For most tests the new device was housed in a titanium package matching the size and two-hole pattern of the traditional flat steel package of the legacy sensor. However, in a side-by-side test described below, the data from the new sensor in the hard-mounted package is compared to the legacy sensor in a much larger mechanically filtered package, both subjected to metal-to-metal hammer conditions.

One of the hammer tests was performed with both sensors in their respective ceramic leadless chip carrier (LCC) packages which were surface mounted to a circuit board. This packaging alternative reduces the footprint by 80% from the original metal package, as shown in Figure 1.
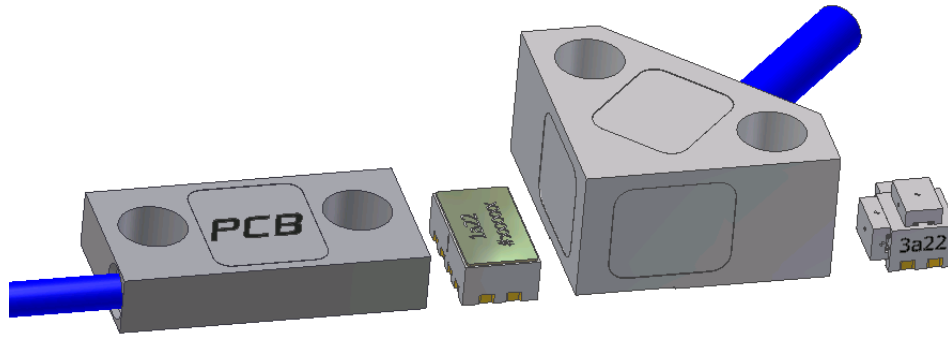
Figure 1. Scaled comparison of packaging configurations, shown approximately three times actual size. At left is the metal case with its cable; next to that is the surface mount ceramic leadless chip carrier with its 80% reduction in footprint. A triaxial configuration is shown with the same mounting hole pattern as the single axis metal case (but with an 8-wire cable.) To the right is the surface mount triax, with its three individual flip chip sensors attached to the orthogonal surfaces of the surface mount ceramic block. Since the new sensor is hermetic, it can serve as its own package. Modification of the MEMS element to a "flip-chip" configuration with solder balls allows solder connections to a circuit board or the surface mount triax block. The footprint of the flip-chipped sensor would be an additional 80% reduction from the surface mount package, or more than a factor of 20 from the original metal package size.

Review of the Sensor

Past designs of MEMS shock sensors emphasized extremely high resonance frequencies. As a result, the nanometer-range displacement of the inertial mass, along with the use of single crystal silicon, resulted in very low damping and correspondingly extreme values of resonant amplification. Users of past designs were forced to choose less sensitive higher range sensors, and in some cases mechanical isolation, to avoid saturation of signal conditioning and data acquisition, and to avoid sensor over-range failures during shock events. Stops and squeeze film damping were incorporated in the new sensor to avoid this weakness [1].

The spacing of components for stops and damping requires extraordinary control of dimensions, made more manageable by designing the displacement at full scale to be of the order of micrometers rather than nanometers. A lower resonance frequency was designed, using a highly symmetric spring-mass system, so that dimensional control could be sufficiently precise to limit travel, prevent damaging stress, regulate air flow and thus control energy dissipation. By design the frequency chosen also satisfied the bandwidth requirements of meaningful measurements in fuzing and pyroshock. [2]

The new sensor is a hermetically sealed sandwich of three silicon layers, Base, Core and Lid, depicted in Figure 2. The middle Core layer holds the "X" shaped mass with four cantilevers, two on its top surface and two below, constraining the mass to planar motion and assuring extremely low transverse sensitivity. The direction of sensitivity is normal to the mounting surface. The Lid and Base layers provide mechanical stops to protect against over-travel of the mass, and grooves in the Lid and Base control the flow of squeezed air and therefore degree of damping.
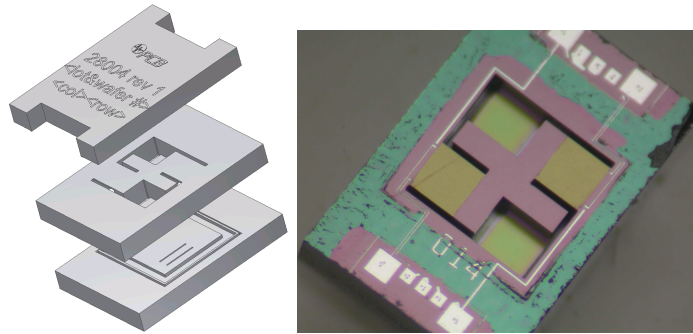
Figure 2. Exploded view of sensor, and a photograph of a core layer extracted from the sandwich. The glass frit used to bond the Base to the Core and the Core to the Lid is the teal-colored residue around the periphery of central area. The four larger aluminum pads are the wirebond pads, and the smaller pads allow in-process trimming of the Zero Measurand Output (ZMO).

Expanding the family to a planned higher-range 60kG version will simply require thicker cantilevers. This will use the same advanced semiconductor processes now employed for the 20kG range, which give the advantages of precise control of dimensions and parameters.
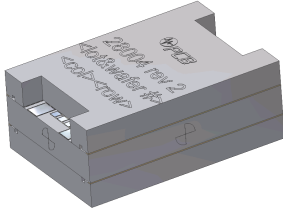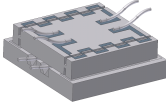
For all ranges, the semiconductor strain gauges are implanted into the top surface of the Core, at locations closest to the rim and the mass for "tension" and "compression" gauges, respectively, in a conventional Wheatstone bridge. The design of the structure and gauges resulted in a Full Scale differential output of the Wheatstone bridge of 2% of the excitation voltage.

Another process used for improved control is the boron implantation, which benefits several performance parameters dealing with the bias error of this dc coupled device. With fully active Wheatstone bridges, the cause of Zero Measurand Output (ZMO or bias) is the degree of mismatching of resistance value of the tension and compression gauges, and Thermal Zero Shift (TZS) is the difference of how the two sets of gauges change over temperature, both of which are a function of the concentration of boron. Uniformity of concentration thus reduces both ZMO and TZS.

The tension and compression gauges on the legacy sensor are on opposite faces of the wafer, so are created by two distinct doping operations. It is more difficult to match opposite sides than devices on the same side of a wafer. The effect of this was demonstrated with warmup tests of both new and legacy sensors in LCCs on a fiberglass circuit board. In a private communication, the new sensor's warmup drift was more than 4 times smaller than that of the legacy sensor.

The performance of the 20kG sensor is listed in Table I, shown alongside the 20kG version of the legacy sensor to which it is compared in the tests discussed later.

Table I. Comparison of 20kG Sensors

	New Sensor	Legacy Sensor
Size	2.5 x 1.7 x 1mm	1.2 x 1.2 0.3mm
Sensitivity	1uV/V/G	1uV/V/G
Resonance	~65 kHz	~350kHz
Resonant amplification "Q"	~10	~1000
Mechanical stops	+/- 40kG	none
Input Resistance	~5000 Ohm	~500 Ohms
Hermetic	yes	no
"Flip-chip" capable?	yes	no

Review of Current Packaging

Figure 1 showed the three current package configurations, all used with the same MEMS sensor. The most common is the conventionally shaped metal package, yet it conceals unconventional design features: the case is low mass, made of titanium, and in the cable all conductors are made of silver coated Kevlar fibers. Pull strength is improved, and mass is reduced compared to the conventional copper conductors. Insulators are noise-treated to reduce triboelectric noise.

Packaging affects performance. The lighter titanium can be more securely constrained by mounting screws than heavier stainless. One potential impact of using titanium is that thermal conductivity of titanium is poorer than stainless steel. This lengthens the time to come to thermal equilibrium, which is one aspect of warm-up drift. However, the new sensor's input resistance is an order or magnitude higher. This means the power which needs to be dissipated through the package (or drawn from batteries) is an order of magnitude lower, so the thermal step that must be attained at equilibrium (and any zero shift associated with that temperature change) is ten times smaller.

Testing

Environmental tests were performed initially at the manufacturer in New York, described in Reference [1], but the tests generally had energy too small to adequately simulate harsh field environments. The following tests were performed at outside facilities with greater testing capabilities.

Hopkinson Bar Tests

The first tests described were performed on a Hopkinson bar with the capability for pulse shaping as well as use of a quartz disk used as a force reference, from which acceleration could be calculated. As shown in Figure 3, the test was performed as a side-by-side comparison with either 20kG and 60kG versions of the legacy sensor. Results of testing at 10kG and 40kG are shown in Figures 4 and 5.
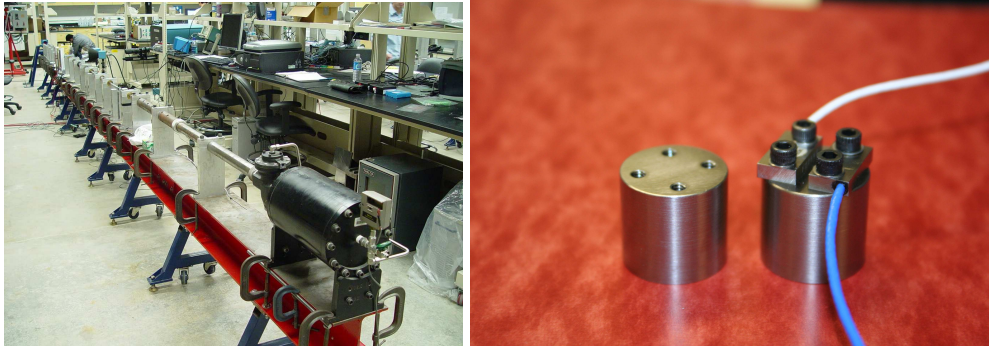
Figure 3. Comparison on Hopkinson bar at Purdue University. The new sensor is placed side-by-side with the legacy sensor on a tungsten flyaway. Photos and data shown in following graphs are courtesy D. Frew and H. Duong of Sandia National Laboratory. [3]

The quartz disk was placed between the end of the bar and the flyaway. The output of the quartz force gauge was scaled by the total mass of the flyaway and sensors as an independent measure of acceleration. That value was overlaid in the graphs, to be compared to that measured by the accelerometers.
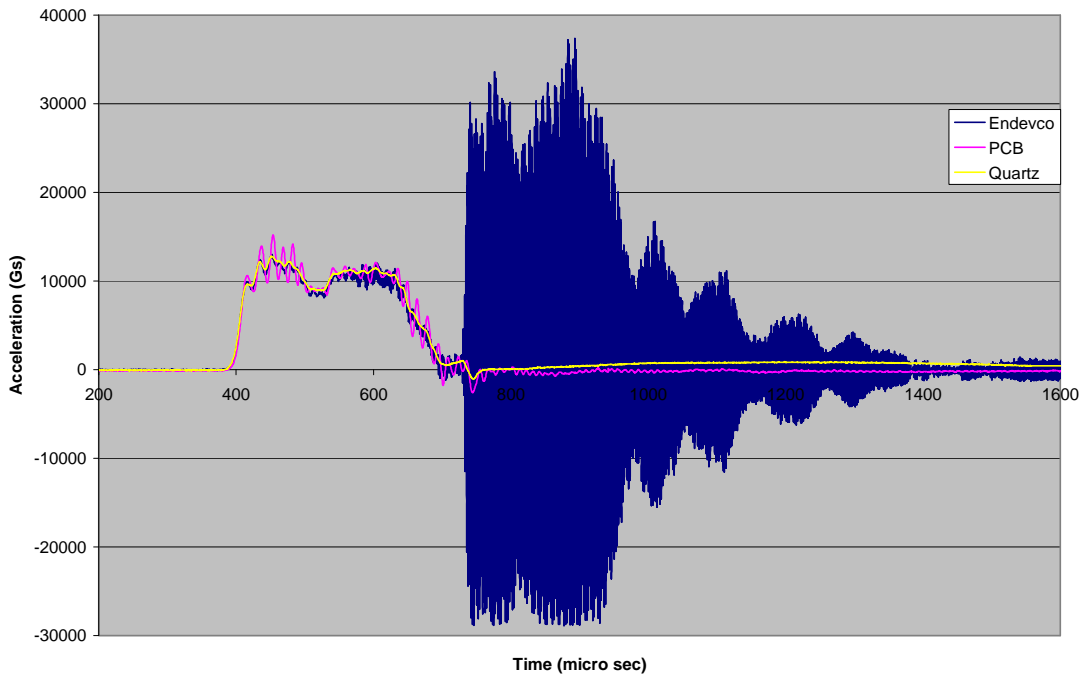
Figure 4. Comparison at 10kG. Low level tests showed good correlation of three sensors. The new sensor showed some low Q resonant amplification during the initial pulse, and the legacy sensor (20kG) showed extremely high Q response after the flyaway fixture detached from the bar. After flyaway separation, some zero shift is observed on the output of the piezoelectric quartz disk.
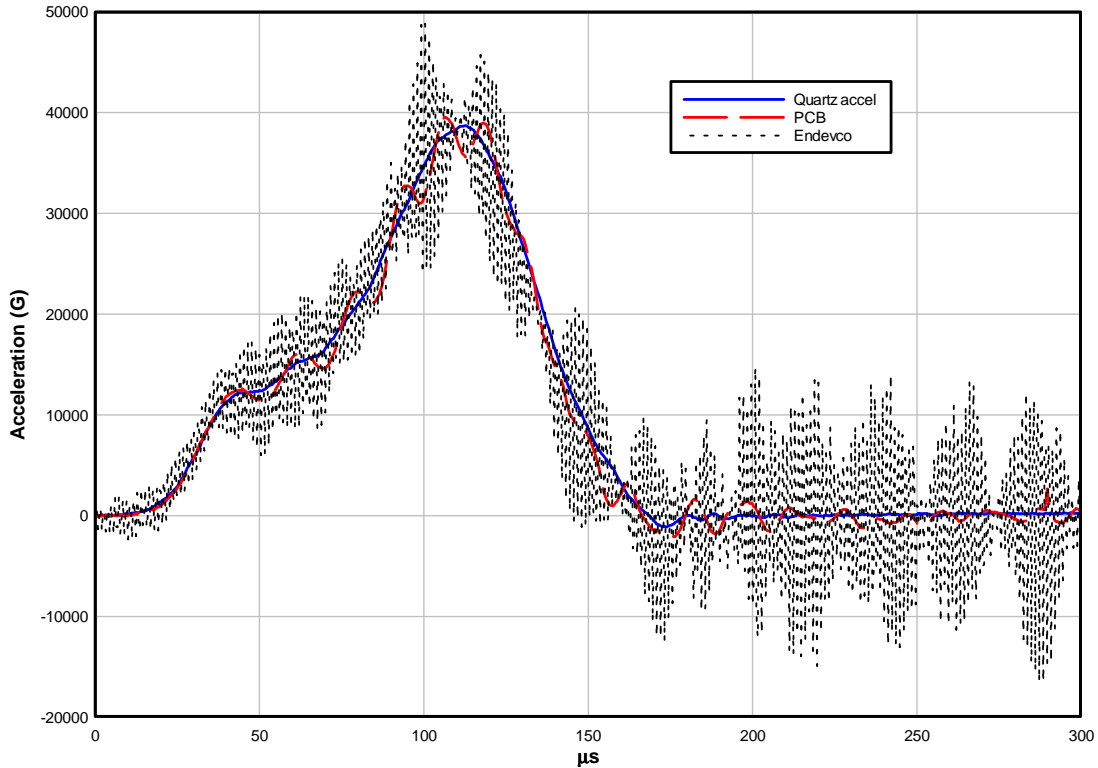
Figure 5. Comparison at 40kG. Wideband data shows ~40kG amplitude was still below stop
levels of the new sensor, and linearity was shown to be good at twice Full Scale. High Q response
of legacy sensor (60kG) is visible throughout the pulse.

Penetration Tests

The drawings of Figure 6 depict the ~100 pound STUBBI penetrator and canister which
was launched at ~850ft/s through a 2 foot thick concrete target at Eglin AFB in Ft.
Walton Beach, Florida. The sensor was mounted in the canister alongside the 60kG
legacy sensor with the batteries and recorders, which stored the entire event of set-back,
penetration and final stoppage in the embankment behind the target. The penetration data
is presented in Figure 7. Preliminary analysis of the new sensor output gave reasonable
set-back and velocity changes, with no indication of zero shifts. All sensors survived the
event, but unfortunately a wire failure in the accompanying legacy sensor's circuit
prevented comparison data.

Figure 6. Configuration for test in STUBBI Penetrator. Two sensors were mounted in an instrumentation canister, along with batteries and recorders packed in glass beads. The recorders were set to 1MHz sample rate and 125kHz antialiasing filter. Illustration courtesy of A. Beliveau of Eglin AFB AFRL.
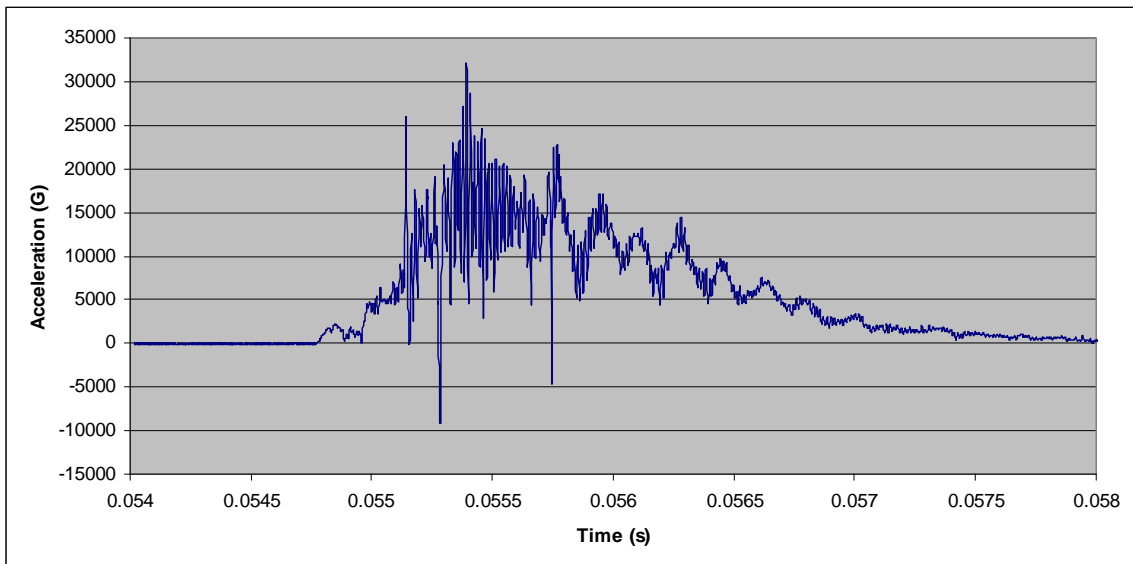

Figure 7. Waveform while penetrating 2 ft concrete. The new sensor's ~65kHz resonance damped quickly to show both the rigid body deceleration causing ΔV of ~750 ft/s during impact and the structural modes of the STUBBI penetrator and instrumentation canister. Data courtesy of J. Foley and A. Beliveau of Eglin AFB AFRL.

Another penetration test was performed at the US Army ERDC, Vicksburg MS. Two recorders were used with three channels each, sampling the outputs of the two triaxial arrangements of the new and legacy sensors at 75kH with 10kHz filters. They were launched at ~1440 ft/s into unreinforced unconfined 6000 psi concrete, stopping within the concrete after 33" of penetration and a peak deceleration of 15kG. The physical configuration is shown in Figure 8 and data in Figure 9.
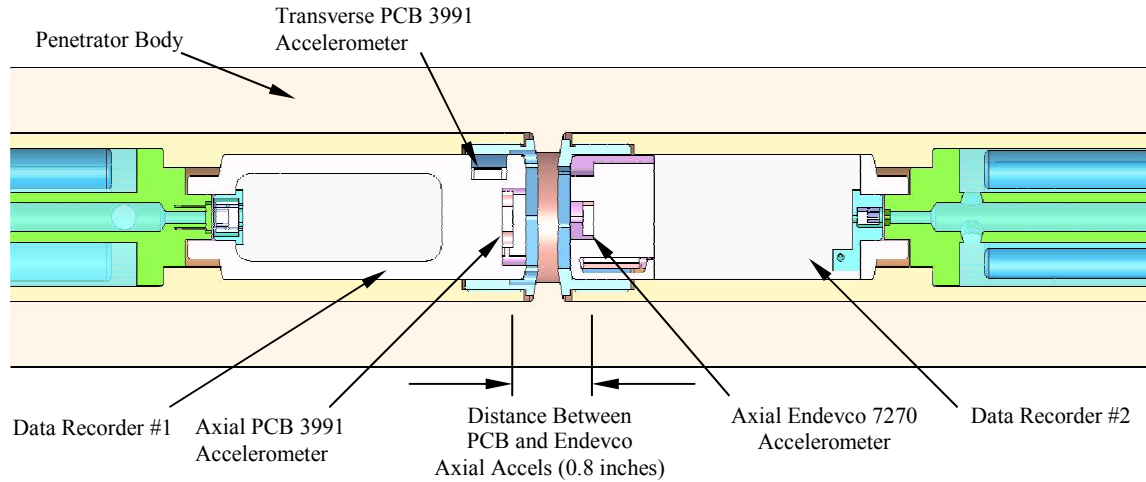
Figure 8. Placement of sensors and recorders. The front of the 3" diameter 30 lb penetrator is at the left. The sensors were closely spaced by the back-to-back arrangement of the canisters so the accelerations would be well correlated. Illustration courtesy of D. Frew, Sandia National Laboratory.
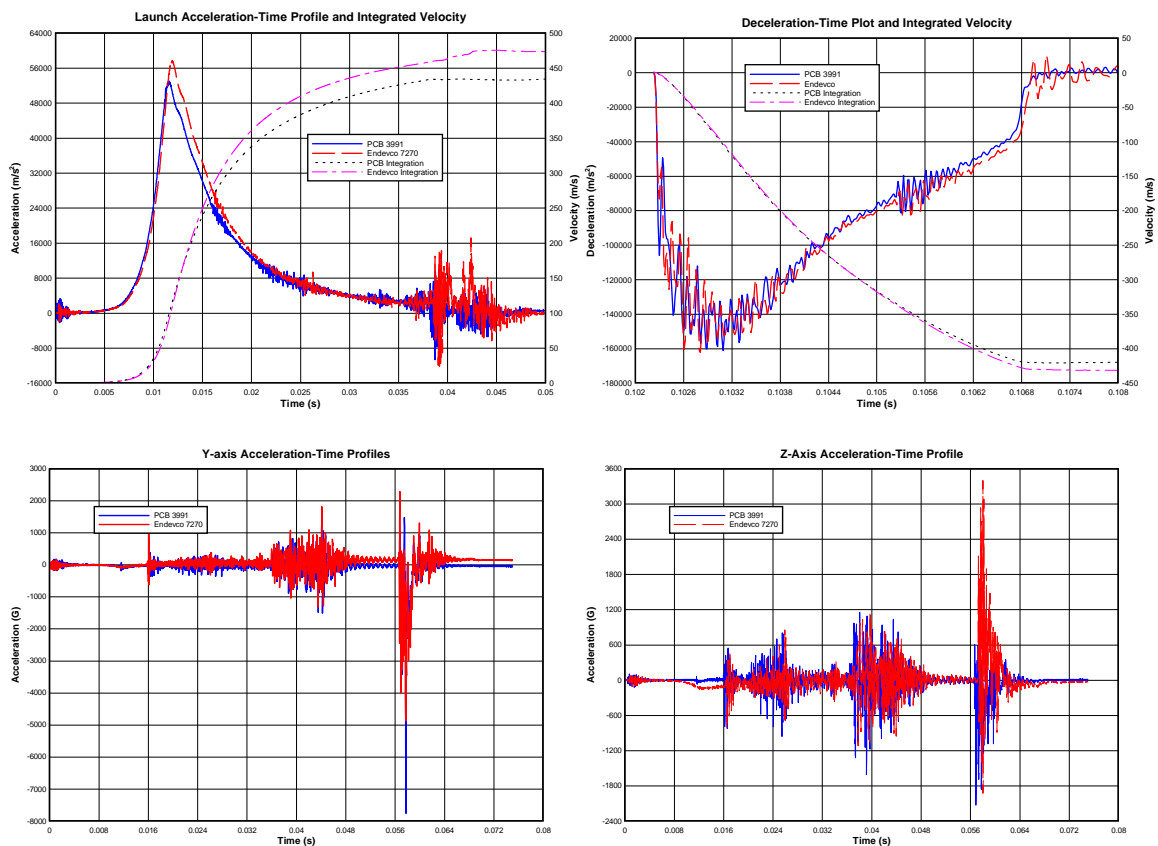

Figure 9. Comparative waveforms of triaxial sensors. Waveforms at upper left and right represent the sensors during launch and impact, respectively, each oriented in the axial direction. The transverse data for the launch are the lower graphs, showing the largest rattle when leaving the barrel. Both legacy sensors in the transverse directions display zero shift. Data is courtesy of R. Hastie, US Army ERDC, Vicksburg MS.

Pyrotechnic Tests

Because of the extremely high frequency content of explosives and the potential of damage by resonant amplification, the legacy MEMS sensor is seldom used in pyrotechnic tests. More commonly used are internal electronic piezoelectric accelerometers, usually with internal electrical filters and often with an additional mechanical filter, which has the form of the internal sensor subassembly suspended by elastomers. Such a device (labeled as "ICP" on the graph) was placed alongside the new MEMS sensor in a near-field explosive test, the results of which are shown in Figure 10.
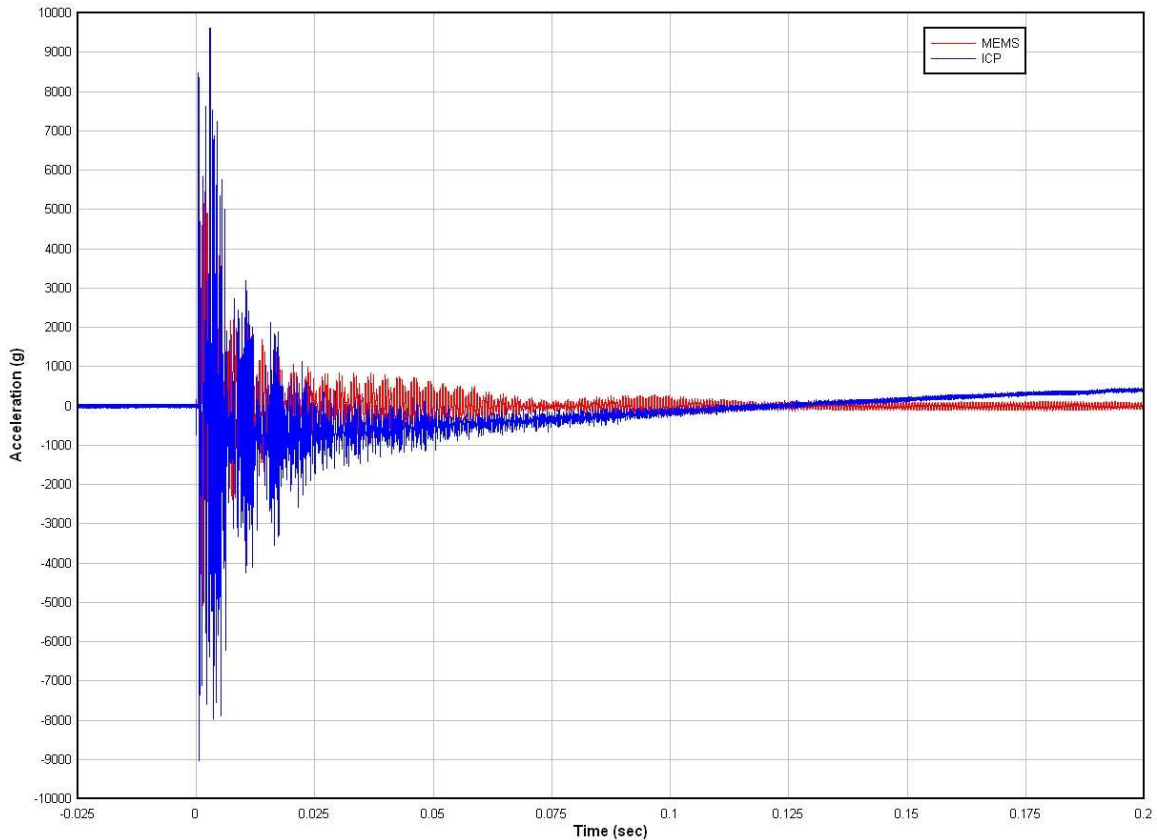

Figure 10. Comparative waveforms of ICP® and MEMS sensors subjected to pyrotechnic blast. The design of the ICP device included both internal electrical and mechanical filters. Its unstable output may indicate unwanted thermal response, displaying a non-zero slope and excursion of hundreds of g's above the initial level. The MEMS sensor stayed flat, as the physics of the event would predict, after the event. Data is courtesy of James Mathis, Southwest Research Institute.

Hammer Tests

Two sets of hammer tests were performed, covering a variety of packaging. In the first set, sensors in side-by-side LCCs surface-mounted to a fiberglass circuit board were powered and operated while on a "VHG" shock machine at its maximum setting of ~90kG. Tests were performed at various temperatures, as low as -54C. Both sensors were reported to survive, with anecdotal observation that resonances were somewhat stronger when cold. (This is supported theoretically, since viscosity of the trapped gas in the new sensor would decrease by ~20% at that temperature.)

Another metal-on-metal hammer test was performed, depicted in Figure 11, side-by-side with one each of 20kG and 60kG versions of the legacy sensor. The new sensor was hard mounted to the test specimen, whereas the legacy sensors were configured in a mechanically filtered housing.
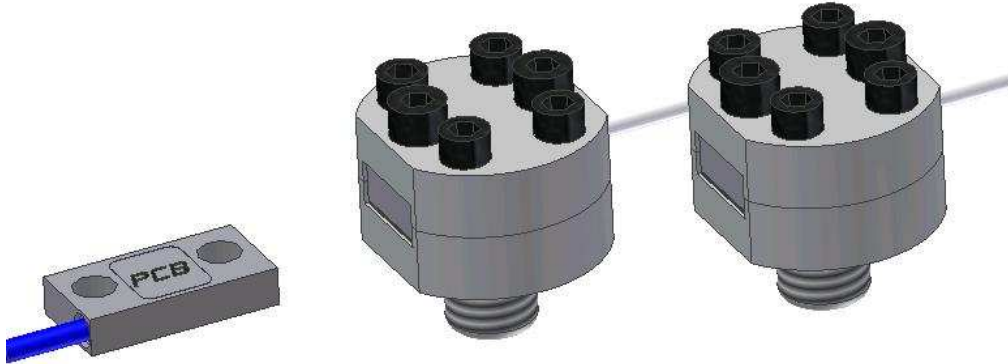

Figure 11. Orientation for hammer tests. This depiction shows the size and approximate separation of the new sensor alongside mechanically-filtered legacy sensors on the test specimen, which is not shown. Point of impact was near the sensors, in a direction normal to the mounting surface, and therefore parallel to the sensitive axis of all sensors. The mechanically filtered package is traditionally used to prevent failure due to Over Range from resonant amplification of high Q legacy sensor during explosive events and metal-to-metal impacts.

The hammer test consisted of approximately 100 blows in rapid succession, with each blow generating peaks at approximately 10kG as measured by the wideband data acquisition (5MHz sampling with 2.5MHz antialias filters). Data is shown in Figures 12-13. Despite the mechanical filtration, the legacy sensors showed considerable high frequency input and their resonance frequencies were excited.
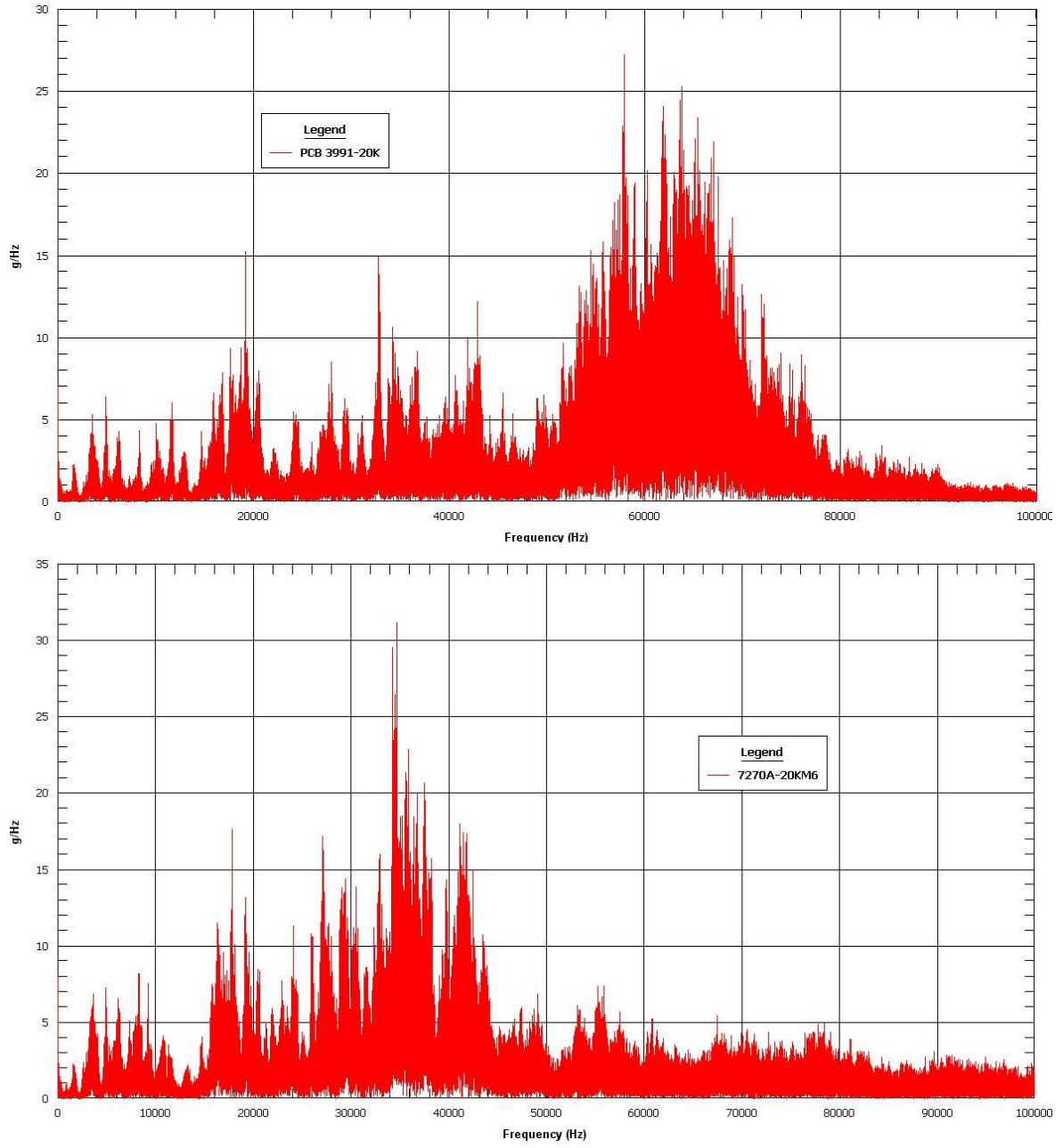
Figure 12. FFT of hammer tests, focusing below 100kHz. Above is the spectrum of the new sensor, showing the ~65kHz low Q resonance. Below is the 20kG legacy sensor, with ~30-40kHz low Q resonance in the housing of the mechanical filter. A similar plot was seen of the 60kG version. For all, the data below 25kHz matched fairly well. The next figure shows higher frequencies.
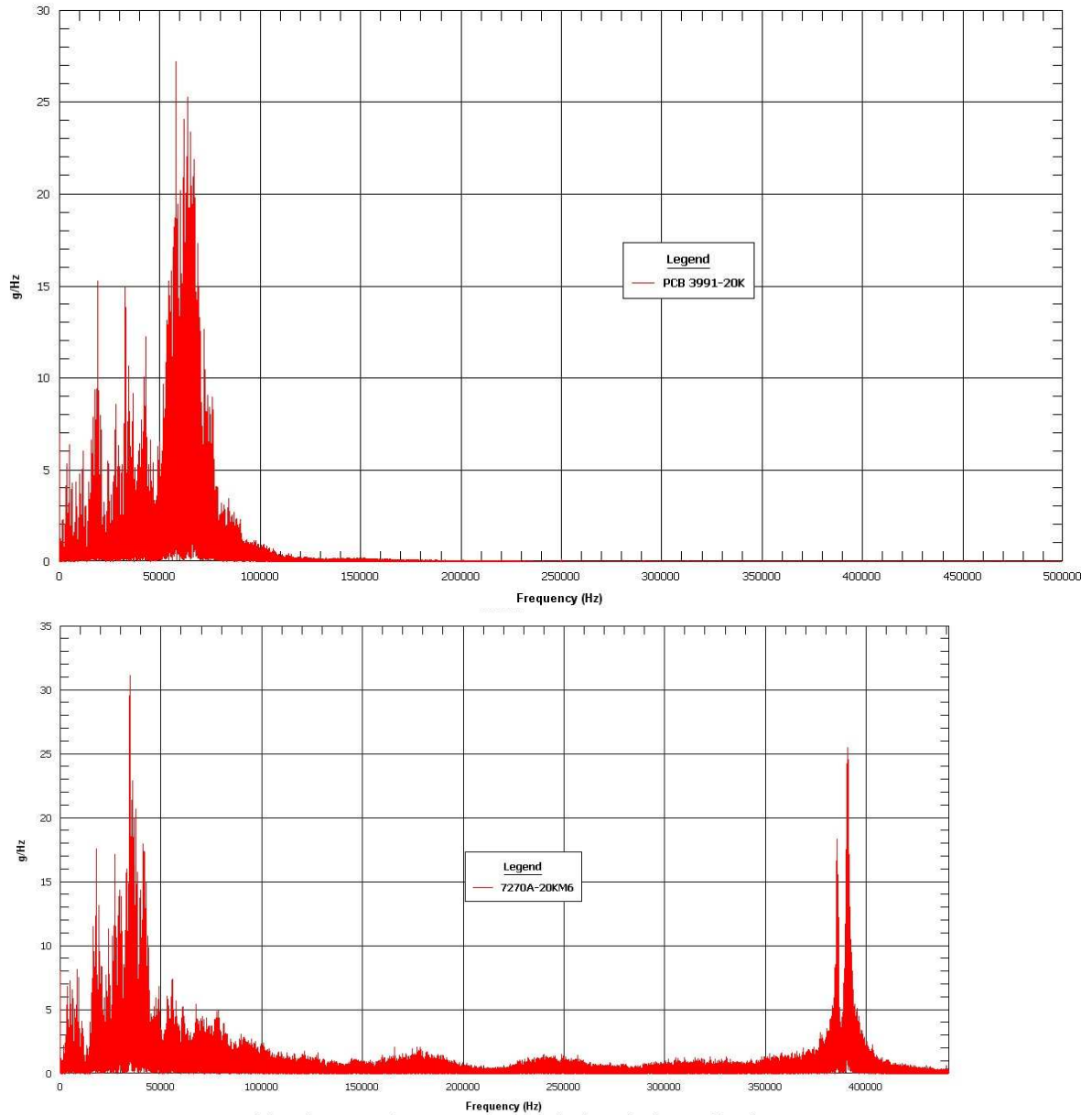
Figure 13. FFT of hammer tests through resonance. This is the same FFT results as in previous figure, but a wider view shows that the new sensor's low resonance and squeeze film damping effectively filtered higher frequency components, whereas the high Q 380kHz twin resonances of the 20kG legacy sensor comes through despite mechanical isolation. A similar plot of the 60kG legacy sensor showed a 900kHz resonance. A more revealing view of the high frequency components of the new sensor is shown in a logarithmic plot in Figure 15.

The preceding data shows that the damping of the new sensor provides effective protection yet delivers data uncorrupted by the mechanical filter used to keep the legacy sensor from resonating to failure. Understanding this damping was the subject of transient and shaker-based tests at the manufacturer, and is presented next.

Damping Tests

In the plot of Figure 14, the transient technique of logarithmic decrement δ was used to determine damping at resonance. The pertinent equations for the classic spring/mass/damper single degree of freedom system [3] are

- $\delta = \ln(x_1/x_2) = 2\pi\, \zeta\, / \,(\mathrm{sqrt}(1\text{-}\zeta^2)) = \zeta\, \omega_n\, \tau = \zeta\, n$
- $\zeta = c/c_c$, where c_c is critical damping
- for $x_1/x_2 = 2$, $\zeta = {\sim}0.11/n$
- $Q = 1/(2\zeta)$

An amplitude decay of a factor of 2 over a period τ is observed over 2.3 oscillations (**n**), and indicates damping of $\zeta = {\sim}0.05$ and $Q = {\sim}10$.
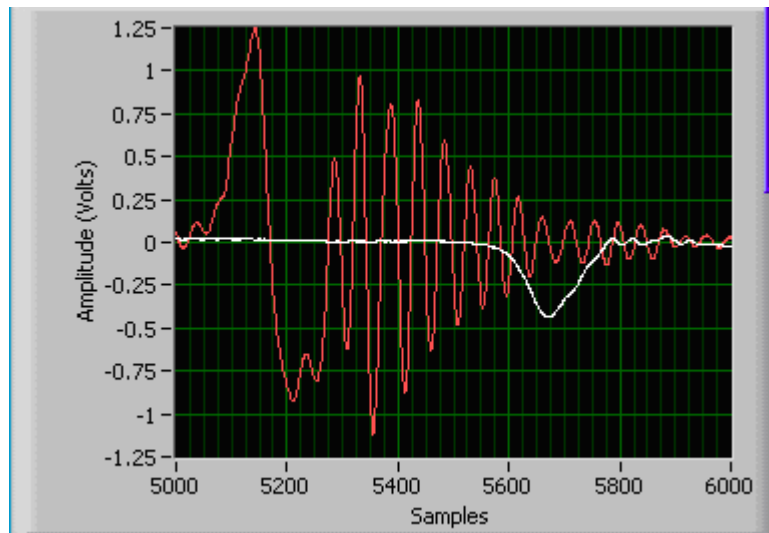

Figure 14. Logarithmic decrement of resonant response in the new sensor. Red trace is sensor resonance output with fast Hopkinson bar pulse, which decays 50% in a period of between 2 and 3 cycles. The white trace is strain gauge on bar. (Credit: T. Jaskolka of PCB Piezotronics Inc.)

Shock sensors in general have sensitivity so low that it is can be difficult to get reliable data from shaker-based sensitivity and phase frequency response data. A quadrature laser interferometer and a beryllium armature air bearing shaker is probably the most capable technique available and was utilized to get the sensitivity and phase data shown in Figure 15. (Credit: J. Dosch and J. Kessler of PCB Piezotronics Inc.)
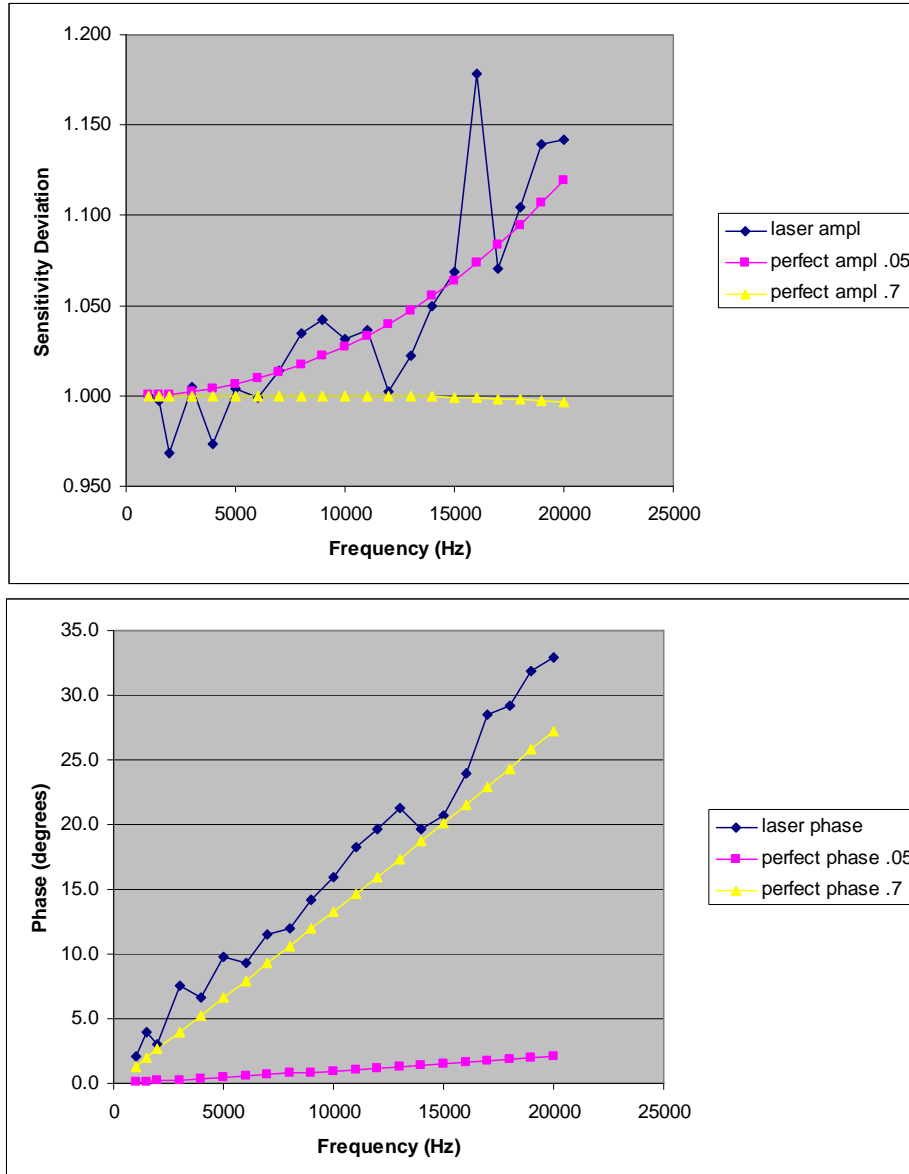
Figure 15. Shaker-based frequency response measurements, referenced to a laser interferometer. Data on sensitivity and phase for one sensor is shown in blue. Also shown are the theoretically perfect responses of a single degree of freedom system with resonance frequency of 61kHz, one with damping coefficient of 0.05 and another with optimally flat 0.7 damping. The sensitivity response at top matches the 5% damping curve, whereas the phase measurements at bottom closely match the "linear phase" of 70% damping. (The linear phase translates to a delay for all frequencies, meaning in this case that the entire waveform of a transient pulse would be shifted 4 microseconds. For comparison, in 4 microseconds the distance traveled by an object moving at Mach 1 would be 1.3 mm.)

This unusual dual nature of damping is probably explained by the non-linear and dual nature of squeeze film damping. That is, as frequency increases, forces involving air transition from being due to viscosity (from flow) to elasticity (from compression) of the air. Elastic forces don't dissipate energy, so damping should decrease above ~10kHz and the effect of the resonance dominates the sensitivity curve. The damping at the resonance

frequency, as determined by transient technique of Figure 14, and as indicated in the hammer test redisplayed in Figure 16, also appears to match a low (~5%) value.
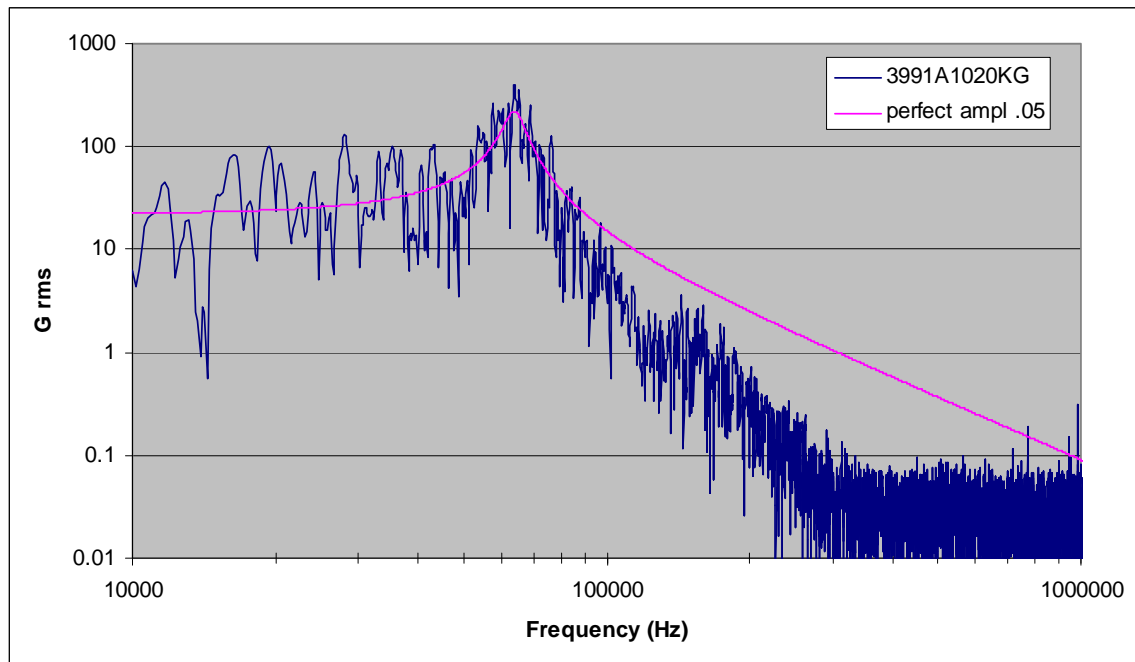

Figure 16. FFT of hammer response. Further analysis of the raw data of the new sensor from Figure 13, this time plotted on a logarithmic scale, indicates a damping coefficient of ~0.05 and no significant modes higher than the resonance.

Assuming that the energy is fairly white (that is, uniform over frequencies), as indicated by the legacy sensor in Figure 12, the FFT of the input should approximately match the frequency response of any sensor subjected to it. The rolloff of the new MEMS sensor past the resonance in Figure 16 has a much steeper decline than a perfect single degree of freedom response. This perhaps indicates that the squeeze film damping in the new sensor is more effective than expected. Such an efficient roll off of output by the sensor would make the requirements for sampling rates and antialiasing filters less demanding.

Conclusions

The new piezoresistive MEMS sensor was designed for severe applications such as concrete penetration, metal-on-metal impacts and pyrotechnic events. The fundamental performance and survivability of the sensor was confirmed by the tests described. In these applications, large high frequency components often mask the more important low frequency data (that is, those components with meaningful correlations to structural motion), which has been described in reference [2] as below ~20kHz. In such applications it is vital to the measurement that there be insignificant zero shift. The tests performed confirmed this to be the case as well.

The sensitivity and range of the new sensor handled rigid body decelerations in simulated and real penetrations, and its resonance frequency and squeeze film damping was shown to provide meaningful data to high frequencies, and linear response to well above the full

scale. Even when hard-mounted, the sensor internally filtered high frequency components which could cause potentially damaging resonant amplification of undamped sensors.

The design has been packaged for drop-in replacement to existing applications, but has the capability of being designed into other configurations such as flip chip mounting for extreme miniaturization and integration into circuit boards.

Because the resonance response of the new sensor has been suppressed by a low level of damping, resolution can be improved in systems which once used the extremely high Q legacy sensor. Whereas configurations for the legacy sensor required excessive "head room", using low gain of conditioning and data acquisition to accommodate resonant amplification, gain settings for the new sensor can be scaled to the measurement. Where the 60kG legacy version is replaced by the 20kG new sensor, an additional factor of three increase in output and therefore resolution will be attained. (A future new sensor with the same sensitivity at the 60kG legacy sensor, which will allow measurement to 100kG in the rare instances that is necessary, would also have damping, so the improved resolution through use of higher gain can still be attained.)

Finally, data acquisition for systems using the new sensor can be simplified, since the sample rate and electrical filter corners to avoid aliasing can be lowered by up to an order of magnitude. In addition, the high input impedance means power consumption by the new sensor is reduced an order of magnitude. Due to this and other design features, warm-up drifts are reduced, further simplifying system design.

References
[1] Sill, R., "Development of a Damped Piezoresistive MEMS High Shock Sensor", 78th Shock and Vibration Symposium, Nov 4-8, 2007, Philadelphia PA.

[2] Walter, P., "How High in Frequency Are Accelerometer Measurements Meaningful?", 79th Shock and Vibration Symposium, Oct. 26-30, 2008, Orlando, FL

[3] white paper by Frew, D., and Duong, H., Sandia National Laboratories, "Performance Evaluation of PCB Model 3991High-G Accelerometer", Feb 5, 2008

[3] Thomson, W., Theory of Vibration with Applications, Prentice Hall, 1972, p29-30.

PCB PIEZOTRONICS
AN AMPHENOL COMPANY

3425 Walden Avenue, Depew, NY 14043 USA

pcb.com | info@pcb.com | 800 828 8840 | +1 716 684 0001

WPL_10_1121